A method for the experimental measurement of bulk and shear loss angles in amorphous thin films

Gabriele Vajente,[1, *] Mariana Fazio,[2] Le Yang,[3] Anchal Gupta,[1]
Alena Ananyeva,[1] Garilynn Billinsley,[1] and Carmen S. Menoni[2, 3]

[1] *California Institute of Technology,*
LIGO Laboratory MC 100-36,
1200 E. California Blvd. Pasadena (CA) USA
[2] *Department of Physics, Colorado State University, Fort Collins, CO 80523, USA*
[3] *Department of Chemistry, Colorado State University, Fort Collins, CO 80523, USA*

(Dated: November 28, 2019)

Brownian thermal noise is a limiting factor for the sensitivity of many high precision metrology applications, among other gravitational wave detectors. The origin of Brownian noise can be traced down to internal friction in the amorphous materials that are used for the high reflection coatings. To properly characterize the internal friction in an amorphous material, one needs to consider the energy losses in the bulk and shear modes. In most of previous works the two loss angles were considered equal, although without any first principle motivation. In this work we show how it is possible to use current state-of-the-art coating ring-down measurement systems to extract the material bulk and shear loss angles. We also show that for titania-doped-tantala, a material commonly used in gravitational wave detector coatings, the experimental data strongly favor a model with two different and distinct loss angles, over the simpler case of one single loss angle.

I. INTRODUCTION

High precision optical metrology relies on high finesse and low loss optical resonant cavities, built with high reflectivity dielectric mirrors. The ultimate limit to the length stability of such cavities is often determined by thermal motion of the cavity components. In many cases, such as in interferometric gravitational wave detectors [1–4], the limit thermal noise comes from the Brownian motion of the dielectric coatings [5], composed of alternating layers of amorphous oxides: silica and titania-doped-tantala for the Advanced GW detectors [6]. The amplitude of Brownian noise can be linked to the material internal friction by use of the Fluctuation-Dissipation Theorem [7, 8]. In the simplest possible approximation the energy lost per cycle due to internal friction is modeled as a fraction of the total elastic energy E stored in the resonator eigen-modes, using one single number usually called the *loss angle* ϕ:

$$\langle \Delta E \rangle_{cycle} = \phi \langle E \rangle \qquad (1)$$

However, even for an amorphous material, the bulk and shear moduli are not equal, and therefore by extension there is no reason to assume that the bulk and shear loss angles have the same value. In computing the thermal noise due to the elastic energy loss in a multilayer coating, one needs to take into account both shear and bulk deformations. The resulting displacement noise depends on the value of both bulk and shear loss angles, each one weighted differently based on the size of the probe beam [9]. Therefore, to have an accurate estimate of the Brownian noise in an optical system, it is important to have a reliable measurement of both loss angles.

———————

* vajente@caltech.edu

The most common technique to measure the loss angle(s) of a thin film is to deposit it on a high quality resonator, and measure the decay time τ of all the eigen-modes. This can be accomplished by exciting the resonator and tracking the oscillation amplitude of each mode over time:

$$A_i(t) = A_0 e^{-t/\tau_i} \qquad (2)$$

Some modes might have excess energy loss due to recoil at the suspension point, but it is generally possible to find a suitable set of eigen-modes that are well decoupled from the environment, and that cover a large range of frequencies. Measuring the decay time of this set of eigen-modes allows probing the value and frequency dependency of the loss angles. For each eigen-mode at a frequency f_i, the decay time τ_i is linked to the coated resonator quality factor Q_i and loss angle ϕ_i by the following relations

$$\phi_i = \frac{1}{Q_i} = \frac{1}{\pi f_i \tau_i} \qquad (3)$$

The loss angle of the coated resonator is related to the total elastic energy loss per cycle, and we can therefore divide it in two terms: a contribution coming from the substrate $\phi_i^{(sub)}$ and a contribution coming from the thin film $\phi_i^{(film)}$. The contribution of each term to the total loss angle is weighted by the amount of elastic energy which is stored in the substrate and in the film, on average:

$$\phi_i^{(coated)} = \frac{E_i^{(sub)}\phi_i^{(sub)} + E_i^{(film)}\phi_i^{(film)}}{E_i^{(sub)} + E_i^{(film)}}$$

$$= (1 - D_i)\phi_i^{(sub)} + D_i\phi_i^{(film)} \qquad (4)$$

where we have introduced the mode dependent *dilution factor* $D_i = E_i^{(film)}/E_i^{(tot)}$. The substrate loss angle can be measured before any film is deposited, and it is usually

assumed to remain unchanged by the deposition process. Therefore the difference of loss angles as measured before and after the film is deposited can be used to extract the loss angle of the material composing the film. We define the *excess loss* of the coated sample as

$$\delta\phi_i = \phi_i^{(coated)} - (1 - D_i)\phi_i^{(sub)} = D_i\phi_i^{(film)} \quad (5)$$

The dilution factors D_i can be computed using finite element simulations of the resonators, knowing the elastic properties of the material, or extracted directly from the change in the eigen-mode resonant frequencies [10]. Since we are interested in measuring the bulk and shear loss angles $\phi_{B,i}$ and $\phi_{S,i}$, we need to modify the model in equation 5 above as follows

$$\delta\phi_i = D_{B,i}\phi_{B,i} + D_{S,i}\phi_{S,i} \quad (6)$$

where we defined the new bulk and shear dilution factors as $D_{B,i} = E_{B,i}^{(film)}/E_i^{(tot)}$ and $D_{S,i} = E_{S,i}^{(film)}/E_i^{(tot)}$, so that $D_i = D_{B,i} + D_{S,i}$. If the elastic properties of the film material (and of the substrate) are known, it is possible to use finite element models to compute the dilution factors. In this paper we describe how it is possible to analyze the resonant mode decay times of a thin film deposited on a silica disk-shaped substrate measured in a Gentle Nodal Suspension [11, 12], and express the film properties in terms of bulk and shear loss angle. Similar analysis were done in the past for films on a cantilever composed of alternating layers of silicon nitride and silica [13], and for films on a disk suspended with a fiber, composed of alternating layers of silica and titania-doped-tantala [14]. We show the result of this analysis for a titania-doped-tantala film as an example, and discuss how the experimental data favor a model with different bulk and shear loss angle over a simpler model with equal loss angles. The material studied here is comparable to what was considered in [14], and we note that the results we obtain are different from those obtained in the previous work. More on this topic in section III. We finally discuss how the measured loss angles impact the estimates of thermal noise for the Advanced LIGO gravitational wave detector.

II. MEASUREMENTS

The substrates used in this work consist of fused silica disks, 75 mm in diameter and 1 mm thick, supported at the center by a *gentle nodal suspension* [11, 12]. All the disk eigen-modes that have null deformation at the disk center are accessible in this system, and have very low recoil losses ($Q^{(sub)} \gtrsim 10^8$). The largest fraction of elastic energy is stored in shear deformation, but depending on the mode shape, in particular on the number of radial nodes, there are non negligible amounts of energy in the bulk deformation, allowing us to disentangle the two contributions.

The gentle nodal suspension allows simultaneous tracking of all modes, providing a measurement of both the frequency and the decay time of each mode. All substrates are characterized prior to coating, to measure the substrate loss angles $\phi_i^{(sub)}$ and the frequency of each mode. A 270-nm-thick film of titania-doped-tantala (27% cation concentration of titania) was then deposited with ion beam sputtering on the substrates. The coated samples were then measured again, to obtain a new set of mode frequencies and decay times. The samples were then subjected to a heat treatment (*annealing*), consisting of a slow ramp up to a target temperature, hold for ten hours, and then a slow ramp down to room temperature. The samples measured for this work have been annealed at 500, 600 and 700°C. The film annealed at 700°C showed signs of micro-crystallization, and therefore the corresponding results are not considered in this work. Ring downs were measured after each heat treatment step, resulting in a set of excess loss angles $\{\delta\phi_i\}$ for the as-deposited samples and the annealed samples.

The film thickness t was measured with ellipsometry, and the relative concentration of titania and tantala was estimated from the measured refractive index and X-ray photoelectron spectroscopy. The material density ρ was estimated with a linear interpolation between the two oxide component densities, weighted with the measured oxide concentration.

The thin film changes the flexural rigidity of the disk, resulting in a shift of all resonant mode frequencies of up to about 10 Hz at frequencies above 20 kHz. We used a finite element analysis (FEA) carried out in COMSOL to find the values of the film material Young's modulus Y and Poisson ratio ν that best reproduce the measured changes in resonant frequencies [15]. Instead of using directly COMSOL in the fit procedure, we first produced a random sampling of the film properties space $[Y, \nu, t, \rho]$ and run a FEA for each point. We then fit a third order polynomial function of Y, ν, t and ρ to the simulated frequency shifts, obtaining a fast semi-analytical model that is accurate within tens of mHz. Using this fast model, we carried out a Bayesian inference analysis [16] to estimate the probability distribution and the confidence intervals for Y and ν. Table I summarizes all the measured parameters of the thin films. The results are dependent on the thickness and density of the film.

In this analysis we assumed that thickness and density are constant, since we do not have yet a measurement of how those film properties change with annealing. This assumption is likely wrong, since changes of density, thickness and refractive index have been observed for other amorphous materials [17, 18]. However, we note that the estimate of Y and ν depends mostly on the product of thickness and density, that is, the surface density of the material. Therefore, even though density and thickness could each vary, if the annealing does not cause any loss of material from the film, we expect that the product of density and thickness will remain constant and the estimate of the Young's modulus and Poisson ratio to be correct. Nevertheless, in the analysis we accounted for possible untracked changes by allowing a ±5% uncertainty in the measured values for both thickness and density.

	As deposited	Annealed 500°C	Annealed 600°C
Young's modulus Y [GPa]	118±3	120±3	128±4
Poisson ratio ν	0.396±0.016	0.407±0.013	0.346±0.019
Cation concentration	73% Ta, 27% Ti		
Thickness t [nm]	268 ± 13		
Density ρ [kg/m^3]	6640 ± 300		

TABLE I. Measured and estimated parameters of the titania-doped-tantala thin film studied in this work. The thickness was measured on the as deposited samples, and the density estimated from the composition. The film elastic properties come from fits to the resonant mode data, as explained in the text. The uncertainties in thickness and density account for possible variations upon annealing, as explained in the main text.

Two samples were coated with nominally equal materials and deposition procedure. The two samples have been measured separately, and the results collated together in all computations.

III. LOSS ANGLE ANALYSIS

For each set of measurements (as deposited samples or annealed samples), we model the excess loss angle either assuming equal or different bulk and shear loss angles for the film material. For both model choices, we allow for a frequency dependency of the loss angles, in the form of a power law or a linear relationship:

$$\phi_{powerlaw}(f; \phi_1, \alpha) = \phi_1 \left(\frac{f}{1 \text{ kHz}} \right)^{\alpha} \tag{7}$$

$$\phi_{linear}(f; \phi_1, m) = \phi_1 \left(1 + m \frac{f - 1 \text{ kHz}}{1 \text{ kHz}} \right) \tag{8}$$

where ϕ_1 is the loss angle at 1 kHz, α is the exponent of the power law, and m the slope of the linear relationship. The excess loss angles measured experimentally are then modeled either with one loss angle, or with different bulk and shear loss angles:

$$\delta\phi_i = D_i \phi_x(f_i; \phi_1, m) \tag{9}$$

$$\delta\phi_i = D_{B,i} \phi_x(f_i; \phi_{1,B}, m_B)$$
$$+ D_{S,i} \phi_x(f_i; \phi_{1,S}, m_S) \tag{10}$$

where x can refer either to the linear or the power law relation, for a total of four different models that could describe the data: single loss angle with linear frequency dependency, single loss angle with power law frequency dependency, bulk and shear loss angles with linear frequency dependency, and bulk and shear loss angles with power law frequency dependency. For each of the four models we use Bayesian inference to estimate the posterior distribution of the parameters, given the model and the measured data. The data consist of the measured excess loss angle for both the samples measured, for each of the accessible resonant mode frequencies. The data likelihood is modeled as a normal distribution, where each data point is an independent random variable with variance given by the experimental uncertainties in the measured quality factors. The prior distributions of all the parameters are flat: the loss angle at 1 kHz can vary in the range $\phi_1 \in [0, 3 \times 10^{-3}]$ for all models; for the power law loss angle models the exponent can vary in the range $m \in [-2, 2]$, while for the linear models the

slope is restricted to values that exclude negative loss angles $m \in [-0.033, 0.5]$.

The posterior distribution of each model's parameters is then sampled using a Markov chain Montecarlo (MCMC) algorithm implemented with the Python package `emcee` [19]. Confidence intervals for each parameters are computed by marginalizing over all other parameters. Figure 1 shows an example of the posterior distribution of the model parameters, given the measured data, for the two samples annealed at 500°C, and considering the following two models: one single loss angle with linear frequency dependency, or bulk and shear different loss angles with linear frequency dependencies (similar results are available for all annealing temperatures and the power law models, but they are not shown here for brevity). The two *corner plots* show the joint probability distribution for pairs of parameters, as well as the probability distribution of each parameter, marginalized over all the others. The dashed lines in the one-dimensional histograms represent the 90% confidence intervals and the median of the posterior distributions.

Once the posterior distribution of all model parameters is computed, we can compute the distribution of the excess loss angle and compare the results with the experimental measurements. Figure 2 shows the results for both model considered here as an example: single loss angle with linear frequency dependency and different bulk shear loss angles, again with linear frequency dependency (similar results for all annealing temperatures and power law frequency dependency are also available, but not shown here for brevity). In those plots the distribution of the excess loss angles are shown and compared with the experimental results. In the case of the bulk and shear loss angle model, both contributions are shown separately, together with the sum. One can notice that most of the excess loss angle is due to the shear contribution, but there is nevertheless a not negligible contribution coming from the bulk losses.

The Bayesian approach we used to fit the model parameters allows us to compute the probability of the different models, given the measured data points. Assuming all models are equally likely a priori, we can compute the logarithm of the Bayesian odd ratio of any pair of models, given the data:

$$\log O(\mathcal{M}_1, \mathcal{M}_2) = \log \left[\frac{P(\mathcal{M}_1 | \delta\phi_i)}{P(\mathcal{M}_2 | \delta\phi_i)} \right] \tag{11}$$
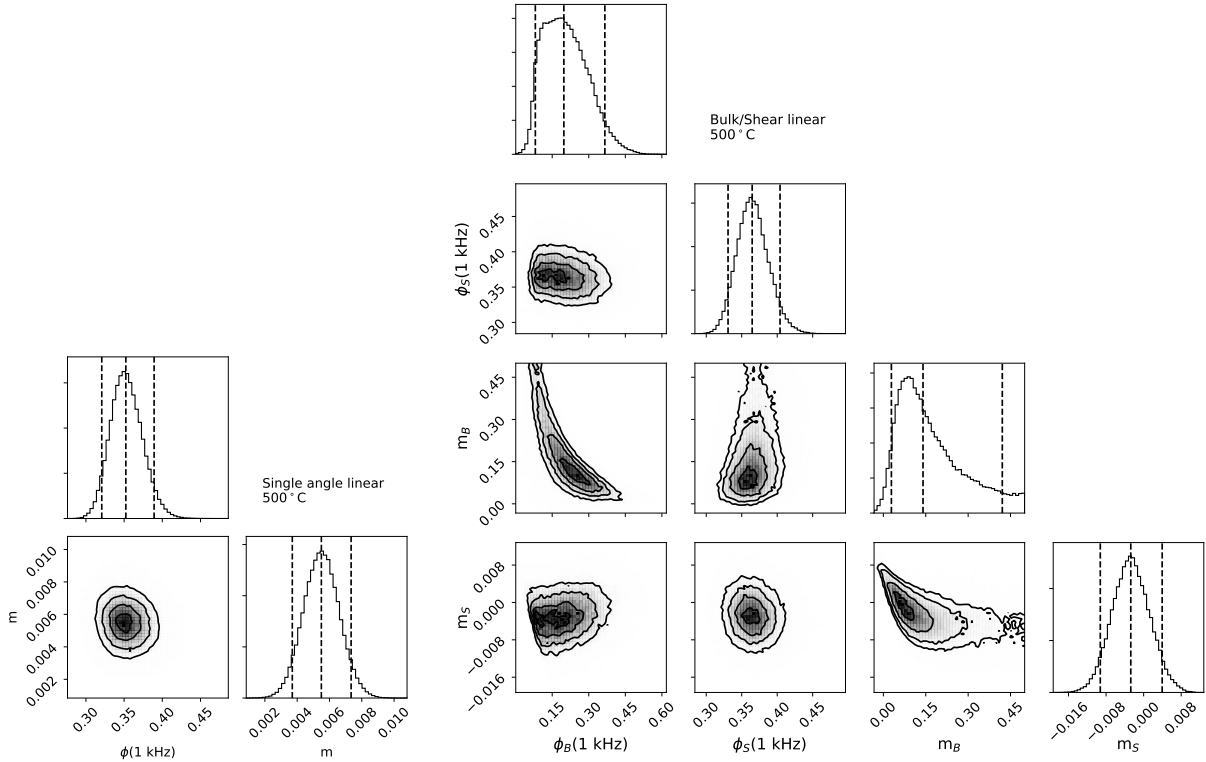
FIG. 1. Posterior probability distributions of the parameters of two loss models (left, one loss angle with linear frequency dependency; right, bulk and shear different loss angles with linear frequency dependency. The results shown here as an example, correspond to the measurements of titania-doped-tantala films after annealing at $500°$C. The posterior probability distributions have been marginalized over the Young's modulus, the Poisson ratio, the film thickness and density.

Model 1	Model 2	As deposited	Annealed 500°C	Annealed 600°C
Model 1	Model 2	As deposited	Annealed 500°C	Annealed 600°C
Single angle, power law	Bulk/Shear linear	-15.5	-6.2	-18.1
Single angle, linear	Bulk/Shear linear	-7.4	-1.6	-10.1
Bulk/Shear power law	Bulk/Shear linear	-0.6	-0.2	-1.8
Single angle, power law	Bulk/Shear power law	-14.9	-6.1	-16.3
Single angle, linear	Bulk/Shear power law	-6.8	-1.4	-8.3

TABLE II. Bayesian odd ratios of the models considered in this analysis. Every table entry shows the logarithm of the Bayes ratio of Model 2 over Model 1. Negative values means that the data favors Model 2. The bulk-shear angle, linear frequency dependency is favored for all annealing temperatures.

where $P(\mathcal{M}_n|\delta\phi_i)$ represents the posterior probability of model $\mathcal{M}_n$ given the measured data $\{\delta\phi_i\}$. A logarithm odd ratio greater than zero means that the measured data favors the model at the numerator $\mathcal{M}_1$, while a value lower than zero means that the model at the denominator $\mathcal{M}_2$ is favored. Table II lists the logarithm of the odd ratio for pairs of models. For all the annealing temperature, as well as for the as deposited film, the measured data strongly favor the models with different bulk and shear loss angles. Among those models, the linear frequency dependency is slightly favored. Table III summarizes the estimated parameters for this model. Figure 3 shows the results in graphical form. In the same plot we compare the bulk and shear loss angles with the estimate obtained using a single loss angle model, as done in most of previous work.

The results for the as-deposited film can be compared with what reported in Abernathy et al. [14], where a similar analysis was performed. Figure 4 compares our results with those reported in in Abernathy et al. [14]. Our results are not consistent with what reported in that work, showing opposite frequency dependencies and different relative amplitude of the two loss angles. The reason is not known at the moment of writing. We should note that the two films, although both being made of about 20% titania doped tantala, were produced by different coaters, and therefore might have different properties.

In this analysis the film is assumed to have uniform thickness and mechanical properties, and to cover the entire substrate surface. The expected variation of the film thickness over the surface is expected to be small.
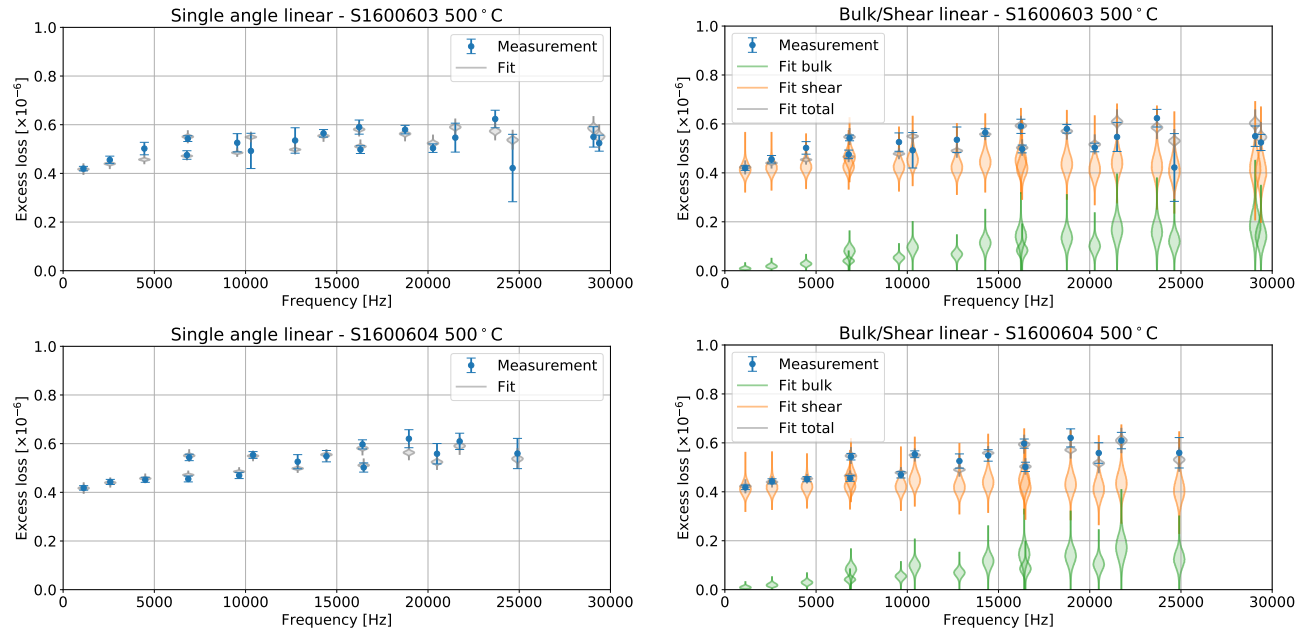
FIG. 2. Comparison of the measured and predicted excess loss angle (not the material loss angle) for the two samples, named S1600603 and S1600604, and shown respectively in the top and bottom rows. The results shown here correspond to the samples measured after annealing at 500°C. The left column shows in grey the distribution of the excess loss angle for the single loss angle model. The right column instead shows the distributions for the bulk and shear loss angle model: in green the bulk contribution, in orange the shear contribution in grey the sum of the two. In both columns, the error bars data points represent the measured values. The violin plots instead represent the distribution of the predicted values, given the result of the Bayesian analysis.

Heat treatment	Bulk loss at 1 kHz $\phi_{1,B}$ $[10^{-3}]$	Bulk loss slope m_B	Shear loss at 1 kHz $\phi_{1,S}$ $[10^{-3}]$	Shear loss slope m_S
30°C	0.19 ± 0.15	0.24 ± 0.19	0.72 ± 0.07	-0.005 ± 0.004
500°C	0.20 ± 0.14	0.14 ± 0.20	0.37 ± 0.04	-0.003 ± 0.007
600°C	0.31 ± 0.11	0.09 ± 0.07	0.26 ± 0.03	-0.012 ± 0.007

TABLE III. Parameters for the best fit to the data in terms of bulk and shear loss angles, with a linear dependency on frequency. The values quoted are the median of the probability distribution of each parameter given the data, and the 90% confidence intervals.

However, variations of the film properties with position might introduce mode-dependent systematic errors that have not been considered in this study. Further work is needed to quantify their effect on the bulk and shear loss angle results.

IV. EFFECT ON THERMAL NOISE ESTIMATE

The standard computations used to estimate the contribution of coating thermal noise in the advanced gravitational wave detectors [5] assume that both the low and high index materials can be described with one single loss angle. Direct thermal noise measurements have also been performed [20] and the results expressed again in terms of equal bulk and shear loss angles. Here we use the result of our analysis, and compute the expected thermal noise for a high reflectivity mirror similar to the design employed in the Advanced LIGO detectors, using the inferred bulk

and shear loss angles. We use the model described in Hong et al. [9].

We consider a high reflection coating composed of 38 alternating layers of silica (low index material) and titania-doped-tantala (high index material), each with an optical thickness of $\lambda/4$ where the laser wave-length λ in vacuum is 1064 nm, to obtain a nominal transmission of about 5 ppm [21]. For the titania-doped-tantala loss angle we use the results reported in this work, for the film measured after annealing at 500°C. We compare two different cases: the best fit to a single loss angle and the best fit with different bulk and shear loss angles, as shown in figure 3. The contribution of silica to thermal noise is small, but nevertheless we included a frequency dependent model obtained from another measurement we performed on silica thin films annealed at 500°C. In this case the sensitivity of our ring-down measurement was not enough to disentangle bulk and shear loss angles: the experimental data is best described by a single loss
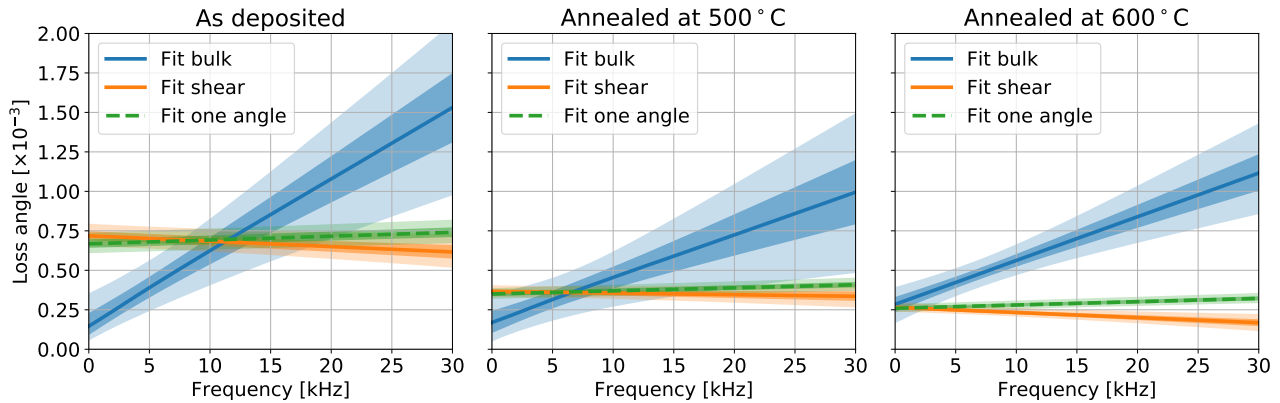
FIG. 3. Estimated loss angles as a function of frequency for the measured titania-doped-tantala film, after each heat treatment step. In each panel, blue and orange shows the best fit to bulk and shear loss angles respectively, while the green dashed line correspond to the best fit to a single loss angle model.
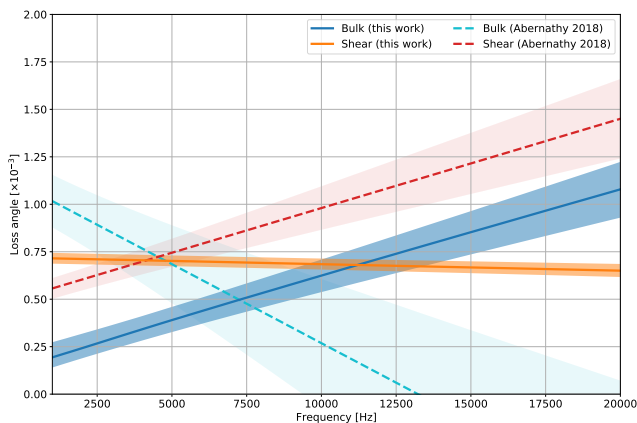

FIG. 4. Comparison of bulk and shear loss angles for the as deposited titania-doped-tantala, as obtained in this work and as reported in Abernathy et al. [14].
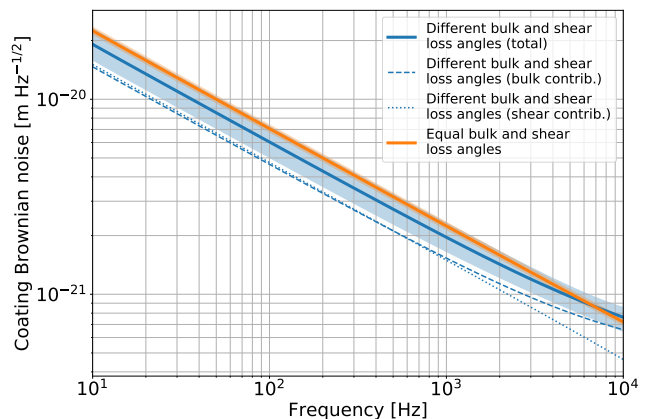

FIG. 5. Brownian noise for a single high reflectivity mirror, composed of alternating layers of silica and titania-doped-tantala, as described in the main text. The solid orange line shows the displacement noise using the model where the bulk and shear loss angles are equal, while the solid blue line corresponds to the model where bulk and shear can assume different values. The dashed and dotted curves show the bulk and shear contribution, respectively.

angle, linearly dependent on the frequency, given by

$$\phi_{SiO_2}(f) = (0.035 \pm 0.004) \times 10^{-3} \cdot$$

$$\left[1 + (-0.006 \pm 0.007) \times 10^{-3} \frac{f - 1 \text{ kHz}}{1 \text{ kHz}} \right]$$

Figure 5 shows the displacement noise due to the Brownian noise of a single high reflectivity mirror. As a reference, assuming the best fit to the data with a single loss angle, we obtain a coating Brownian noise of $(7.0 \pm 0.3) \times 10^{-21}$ m/$\sqrt{\text{Hz}}$ at 100 Hz. Using instead the best fit to the data with different bulk and shear loss angles, we obtain $(6.0 \pm 1.1) \times 10^{-21}$ m/$\sqrt{\text{Hz}}$ at 100 Hz. For comparison, the direct thermal noise measurement reported in [20] can be extrapolated to a level of $(7.5 \pm 0.1) \times 10^{-21}$ m/$\sqrt{\text{Hz}}$ at 100 Hz. Within the precision of our measurement, there is no significant impact on the estimate of thermal noise for and Advanced-LIGO-like high reflectivity coating.

It is worth noting that the knowledge of the separate bulk and shear loss angles could allow an additional degree of freedom to optimize the thermal noise of the coating, by changing the thickness of the layers [9].

V. CONCLUSIONS

We showed that it is possible to estimate the bulk and shear contribution to the loss angle of a thin film, using measurements of the decay time of the resonant modes of a coated silica disk, carried out in a Gentle Nodal Suspension system. As an example we analyzed a thin film of titania-doped-tantala, one of the material used in the advanced gravitational wave interferometric detector mirrors. A Bayesian analysis of the experimental data shows that a model featuring different bulk and shear loss

angle is favored with respect to a simpler model with one single loss angle (i.e. same loss angle for bulk and shear energies). The change in loss angles with annealing is more evident in the shear than in the bulk contribution. When the two models are used to compute the expected thermal noise for a high reflection mirror similar to those used in Advanced LIGO, the difference is marginal and within error bars when the measurements are extrapolated in the frequency region between 10 and 1000 Hz.

[1] J Aasi and others [LIGO Scientific Collaboration]. Advanced LIGO. *Class. Quantum Grav.*, 32:074001, 2015.
[2] B. Willke, B. et al. The GEO 600 gravitational wave detector. Class. Quantum Grav. 19, 1377-1387 (2002)
[3] Somiya. K and others [KAGRA collaboration]. Detector configuration of KAGRA - the Japanese cryogenic gravitational-wave detector. *Class. Quantum Grav.*, 29:124007, 2011.
[4] F Acernese and others [Virgo Collaboration]. Advanced Virgo: a 2nd generation interferometric gravitational wave detector. *Class. Quantum Grav.*, 32:024001, 2015.
[5] Harry, G.M., Gretarsson, A.M., Saulson, P.R., and others. Thermal noise in interferometric gravitational wave detectors due to dielectric optical coatings. Classical and Quantum Gravity, 19(5), (2002) p.897
[6] M. Granata, et al. Amorphous optical coatings of present gravitational-wave interferometers arXiv:1909.03737 [physics.ins-det]
[7] H.B. Callen and T.A. Welton Irreversibility and Generalized Noise Physical Review. 83: 34?40 (1951)
[8] Y. Levin Internal thermal noise in the LIGO test masses: A direct approach Phys. Rev. D 57, 659 (1998)
[9] T. Hong, et al. Brownian thermal noise in multilayer coated mirrors Phys. Rev. D 87, 082001 (2013)
[10] T. Li, et al. Measurement of mechanical thermal noise and energy dissipation in optical dielectric coatings Phys. Rev. D 89, 092004 (2014)
[11] E. Cesarini et al. A gentle nodal suspension for measurements of the acoustic attenuation in materials. *Rev. Sci. Instrum.*, 80, 053904 (2009)
[12] G Vajente et al. A high throughput instrument to measure mechanical losses in thin film coatings Rev. Sci.

Instrum., 88:073901, (2017)
[13] H.-W. Pan, et al. Silicon nitride and silica quarter-wave stacks for low-thermal-noise mirror coatings Phys. Rev. D 98, 102001 (2018)
[14] M. Abernathy et al., Bulk and shear mechanical loss of titania-doped tantala Physics Letters A, 382, 2282-2288 (2018)
[15] M. Granata, et al. Amorphous optical coatings of present gravitational-wave interferometers arXiv:1909.03737
[16] A. Gelamn, J. B. Carlin, H. S. Stern, D. B. Dunson, A. Vehtari, D. B. Rubin Bayesian Data Analysis, 3rd edition Chapman and Hall/CRC (2013)
[17] M. Bischoff et al. Postdeposition treatment of IBS coatings for UV applications with optimized thin-film stress properties Applied Optics 53, A212-A220 (2014)
[18] J. T. Brown Center wavelength shift dependence on substrate coefficient of thermal expansion for optical thin-film interference filters deposited by ion-beam sputtering Applied Optics 43, 4506-4511 (2004)
[19] D. Foreman-Mackey, D. W. Hogg, D. Lang and J. Goodman emcee: The MCMC Hammer arXiv:1202.3665 [astro-ph.IM]
[20] S. Gras and M. Evans, Direct measurement of coating thermal noise in optical resonators Phys. Rev. D 98, 122001
[21] A. Amato et al., High-Reflection Coatings for Gravitational-Wave Detectors: State of The Art and Future Developments J. Phys.: Conf. Ser. 957 012006 (2018)